Carbohydrate Polymers 155 (2017) 425–431

Contents lists available at ScienceDirect

Carbohydrate Polymers

journal homepage: www.elsevier.com/locate/carbpol

Bacterial cellulose nanocrystals produced under different hydrolysis conditions: Properties and morphological features

Niédja Fittipaldi Vasconcelos[a], Judith Pessoa Andrade Feitosa[a], Francisco Miguel Portela da Gama[b], João Paulo Saraiva Morais[c], Fábia Karine Andrade[d], Men de Sá Moreira de Souza Filho[d], Morsyleide de Freitas Rosa[d,*]

[a] Federal University of Ceará (UFC), Department of Chemical, Bloco 940, 60455-760 Fortaleza, Ceará, Brazil
[b] Centre of Biological Engineering – CEB, Institute for Biotechnology and Bioengineering (IBB), Department of Biological Engineering, University of Minho, Campus de Gualtar, 4710-057, Braga, Portugal
[c] Embrapa Cotton – CNPA, Rua Oswaldo Cruz 1143, Centenário, 58428-095 Campina Grande, Paraíba, Brazil
[d] Embrapa Tropical Agroindustry – CNPAT, Rua Dra Sara Mesquita 2270, Planalto do Pici, 60511-110 Fortaleza, Ceará, Brazil

ARTICLE INFO

Article history:
Received 18 March 2016
Received in revised form 18 August 2016
Accepted 26 August 2016
Available online 28 August 2016

Keywords:
Hydrolysis
Sulfuric acid
Hydrochloric acid
Cellulose nanocrystals
Bacterial cellulose

ABSTRACT

Bacterial cellulose (BC) is a polymer with interesting physical properties owing to the regular and uniform structure of its nanofibers, which are formed by amorphous (disordered) and crystalline (ordered) regions. Through hydrolysis with strong acids, it is possible to transform BC into a stable suspension of cellulose nanocrystals, adding new functionality to the material. The aim of this work was to evaluate the effects of inorganic acids on the production of BC nanocrystals (BCNCs). Acid hydrolysis was performed using different H_2SO_4 concentrations and reaction times, and combined hydrolysis with H_2SO_4 and HCl was also investigated. The obtained cellulose nanostructures were needle-like with lengths ranging between 622 and 1322 nm, and diameters ranging between 33.7 and 44.3 nm. The nanocrystals had a crystallinity index higher than native BC, and all BCNC suspensions exhibited zeta potential moduli greater than 30 mV, indicating good colloidal stability. The mixture of acids resulted in improved thermal stability without decreased crystallinity.

1. Introduction

Cellulose is the most abundant renewable biopolymer produced in the biosphere and is obtained mainly from vegetables (plants and some algae species) and microbes (bacteria) (Qui & Hu, 2013). Irrespective of the source, cellulose has the same chemical composition but may bear a different structural organization and, therefore, different physical properties (Brown, 1886; Ross, Mayer, & Benziman, 1991).

Plant cellulose (PC) is usually associated with other biopolymers including hemicellulose and lignin. Depending on the plant source, the extraction process may require corrosive chemicals that are hazardous to the environment, resulting in high economic, environmental, and social costs. Unlike PC, bacterial cellulose (BC; mainly produced by members of the *Gluconacetobacter* genus) is obtained by fermentation. In addition, it is mixed only with microbial cells, nutrients, and other secondary metabolites that can be removed through a mild alkali treatment, yielding highly pure cellulose (Gea et al., 2011; Pecoraro, Manzani, Messaddeq, & Ribeiro, 2008, Chapter 17).

BC has attracted the attention of the scientific community due to its unique characteristics such as high porosity, high water retention capacity, high mechanical strength in the wet state, low density, biocompatibility, non-toxicity, and biodegradability. These features make BC an outstanding material that is suitable for technological applications, particularly in the fields of biomedicine and pharmacology (Czaja, Krystynowicz, Bielecki, & Brown, 2006; Hu et al., 2014; Klemm, Schumann, Udhardt, & Marsch, 2001; Svensson et al., 2005; Shah, Ul-Islam, Khattak, & Park, 2013).

The high purity and crystallinity of BC make it a promising starting material for extracting cellulose nanocrystals (CNCs). CNCs (or cellulose whiskers) are defined as structures with at least 1 dimension in the nanoscale (1–100 nm), and they can serve as building blocks for a variety of applications (Charreau, Foresti, & Vázquez, 2013). In the field of nanotechnology, the *top-down* approaches (e.g.: homogenization, hydrolysis, combined chemical-mechanical processes) can be applied to resize the natural cellulose fibers in

* Corresponding author.
E-mail address: morsyleide.rosa@embrapa.br (M.d.F. Rosa).

http://dx.doi.org/10.1016/j.carbpol.2016.08.090
0144-8617/

small particles as CNCs suspensions, adding versatility and new resources to this cellulosic material.

Acid hydrolysis is the most commonly used method for producing CNCs (Dufresne, 2012, Chapter 3). With this approach, hydrogen ions (H^+) penetrate amorphous cellulose molecules promoting cleavage of glycosidic bonds, thus releasing individual crystallites. Depending on the cellulose source and, especially, the hydrolysis reaction conditions (i.e., the acid type and concentration, reaction time, and temperature), nanostructures with different physical and mechanical properties can be yielded.

Strong inorganic acids, such as H_2SO_4 and HCl, are most commonly used for the acid hydrolysis of cellulose. HCl generates low-density surface charges on the CNC with limited nanocrystal dispersibility, which tends to promote flocculation in aqueous suspensions. In contrast, when H_2SO_4 is used, a highly stable colloidal suspension is produced because of the high negative surface charge promoted by sulfonation of the CNC surface. However, the presence of sulfate groups ($-OSO_3^-$) reduces the thermostability of the nanocrystals (Martinez-Sanz, Lopez-Rubio, & Lagaron, 2011). Some reports describe the concomitant use of H_2SO_4 and HCl to produce stable and thermally resistant CNC suspensions (Corrêa, Teixeira, Pessan, & Mattoso, 2010).

High acid concentrations can be used to hydrolyze both the amorphous and crystalline regions of cellulose. In addition, prolonged hydrolysis times and higher temperatures cause reduced crystallinity and changes in the morphological characteristics and physical properties of the nanocrystals (Dufresne, 2012).

Currently, plants represent the most commonly used source of cellulose for CNC production. Several reports have described the extraction of PC nanocrystals (PCNC) from agroindustrial biomasses such as linter, cotton, coconut fibers, and banana pseudostems (Corrêa et al., 2010; Morais et al., 2013; Ng et al., 2015; Pereira et al., 2014; Qiao, Chen, Zhang, & Yao, 2016; Rosa et al., 2010).

The high energy consumption needed to obtain PCNC sources (1800–94,356 kJ/g of nanocrystals) (da Silva Braid et al., 2015; de figueirêdo et al., 2012; do Nascimento et al., 2016) has boosted research focused on developing new processes with reduced costs and identifying new, feasible cellulose sources. Some studies have investigated the production of BC nanocrystals (BCNCs) by acid hydrolysis using different reaction conditions (George, Ramana, Sabapathy, Jagannath, & Bawa, 2005; George, Ramana, Bawa, & Siddaramaiah, 2011; Martinez-Sanz, Lopez-Rubio, & Lagaron, 2011; Moreira et al., 2009; Roman & Winter, 2004).

In this study, we aimed to investigate the influence of the acid type/concentration and reaction time on the morphology, crystallinity, and thermal stability of nanocrystals obtained from BC. First, we evaluated the effect of H_2SO_4 hydrolysis. Then, based on the results of this experiment, a hydrolysis condition that generated BCNC suspensions with a high module for zeta potential (high colloidal stability) was selected and used to investigate the effects of HCl on the thermal properties of sulfated BCNCs.

2. Materials and methods

2.1. Materials

BC (nata de coco) was obtained from HTK Food Co., Ltd. (Ho Chi Minh City, Vietnam).

The chemicals sodium hydroxide (NaOH), sulfuric acid (H_2SO_4), and hydrochloric acid (HCl) were obtained from VETEC (Rio de Janeiro) and used without further purification and as received from the supplier.

Table 1
Acid hydrolysis reaction conditions used to obtain BCNCs.

Sample	[H_2SO_4] (%, w/w)	[HCl] (%, w/w)	**Time (min)**
BCNC–1	50	–	60
BCNC–2	50	–	120
BCNC–3	60	–	60
BCNC–4	65	–	120
BCNC–3/HCl	34[a]	24[a]	60

[a] These values indicate the real concentrations of the acids in the reaction medium and takes into account the dilution caused by the use of HCl P.A (37.5%, w/w), which has a high percentage of water.

2.2. Methods

2.2.1. Preparation of BC

BC pellicles were maintained in 0.4% NaOH (w/v) at room temperature for 24 h, followed by washing with distilled water until neutralization to remove any chemicals used in the nata de coco-preparation process. Then, the BC pellicles were cut into small cubes (5 mm^3) and processed in an Ultra-Turrax homogenizer (IKA–werne/T50 basic/S50N–G45G) at 5000 rpm for 5 min to obtain a cellulosic pulp. This slurry was filtered through quantitative filter paper (8 μm) and lyophilized. The dried BC was ground using an analytical mill (IKA-werne/A11) and stored in a glass container.

2.2.2. Production of BCNCs

H_2SO_4 and HCl were used to obtain BCNCs. Four acid hydrolysis conditions (designated as BCNC–1 to BCNC–4) involving only H_2SO_4 were used to evaluate the influence of the acid concentration and reaction time on BCNC production, with BCNC–4 serving as the reference condition, as tested by Moreira et al. (2009).

Based on the results of this experiment, one of the tested hydrolysis conditions resulting in a higher module for the zeta potential (BCNC–3) was selected and used to investigate the effects of added HCl on BCNC production (BCNC–3/HCl). The hydrolysis conditions tested in this study are described in Table 1.

For each experiment, 0.6 g of dried BC and 60 mL of acid solution (1:100 ratio, w/v) were mixed at 45 °C with magnetic stirring (500 rpm).

Hydrolysis reactions were stopped by diluting the reactions 15-fold with cold deionized water (15:1 ratio, v/v). Each suspension was centrifuged at 26,400 x *g* (13,000 rpm) for 15 min at 20 °C to precipitate the CNCs. The CNCs were then washed with deionized water and centrifuged again at 26,400 x *g* (13,000 rpm) for 15 min at 20 °C. The resulting suspension was ultrasonicated for 3 min (Unique/Desruptor 60 kHz; 300 W). The centrifugation and ultrasonication steps were repeated 3 times. Finally, the BCNC suspension was dialyzed in deionized water to neutral pH and the final concentration was ~1% w/v.

2.3. Characterization

2.3.1. Zeta potential

The zeta potential of BCNC suspensions at 1% (w/v) (pH = 7) were measured using a Zetasizer Nano ZS (Malvern Instruments Ltd., Worcestershire, United Kingdom).

2.3.2. Thermogravimetric analysis (TGA)

Thermogravimetric (TG) curves were generated in a STA 6000 analyzer (PerkinElmer Instruments; Shelton, USA). The samples (≅ 11 mg) were heated from 50 °C to 800 °C at a heating rate of 10 °C/min in a synthetic air atmosphere (40 mL/min). The derivative thermogravimetric (DTG) curve was expressed as the mass variation as a function of temperature.

Table 2
Results from zeta potential, TGA, and XRD measurements of native BC and BCNCs produced under different acid hydrolysis conditions.

Sample	Zeta potential (mV)	TGA		XRD	
		Temperature *Onset* (°C)	Residual mass (%)	Crystallinity Index (%)	Crystallite size (nm)
BC	n.d.	335	0.77	79	6.39
BCNC–1	−33.6 ± 1.5	223	0.42	91	5.93
BCNC–2	−36.3 ± 1.1	224	0.02	92	5.92
BCNC–3	−53.6 ± 0.7	218	0.63	89	5.78
BCNC–4	−24.7 ± 2.1	164	0.14	22	5.11
BCNC–3/HCl	−43.9 ± 0.8	263	0.14	83	5.22

n.d.: not determined.

2.3.3. X-ray diffraction (XRD)

XRD patterns of samples were performed in an X'Pert PRO MPD X-ray diffractometer (PANalytical, Eindhoven, The Netherlands) using a copper (Cu) tube (λ = 1.5406 Å) at 40 kV and 50 mA. Samples were examined with a scanning angle of 2θ from 10° to 50° at a rate of 1°/min. The crystallinity index (CrI) was calculated as a function of the maximum intensity of the diffraction peak from the crystalline region (I_{200}), at an angle of 2θ ~ 22.5°, and the minimum intensity from the amorphous region (I_{am}), at an angle of 2θ ~ 18°, as described by Segal, Creely, Martin, & Conrad (1959) (Eq. (1)).

$$CrI(\%) = (I_{200} - I_{am})/I_{200} \quad (1)$$

The crystallite size (CS) refers to the average crystal width (I_{200} in this case) and was calculated using Scherrer's equation (Eq. (2)):

$$CS = K\lambda/FWHMCos\theta \quad (2)$$

where K is a dimensionless factor dependent upon the method used to calculate the amplitude (K = 0.94 in this study), λ is the wavelength of the incident X-ray (λ = 0.15416 nm), FWHM is the width of the diffraction peak at half-maximal height (in radians), and θ is the angle of the diffraction peak of the crystalline phase (Bragg's angle).

2.3.4. Differential scanning calorimetry (DSC)

Curves were obtained by DSC using an Q20 DSC (TA Instruments; New Castle, USA). Samples (≅4 mg) were heated from −50 °C to 400 °C under a nitrogen atmosphere (50 mL/min) at a heating rate of a 10 °C/min to evaluate the thermal stability. Variation in the amount of energy absorbed from the cellulose decomposition reaction (ΔH_d) was calculated as the integral of the exothermic peak areas using TA Analysis software.

2.3.5. Fourier-transform infrared spectroscopy (FTIR)

Samples were examined using a 670-IR FTIR instrument (Varian; Mulgrave, Australia). Samples were ground and pelletized using KBr (1:100, w/w), followed by uniaxillary pressure. Spectra were obtained between 4000 and 400 cm^{-1} at a resolution of 4 cm^{-1}.

2.3.6. Electron microscopy

BC pellicles were cut into thin layers (2 × 5 × 1 mm), dried at 50 °C, placed in a stub, and sputter-coated with platinum. Images were obtained in a DSM 940 A scanning electron microscope (SEM; Zeiss, Germany) with an acceleration voltage of 15 kV.

CNC suspensions were sonicated for 15 min, and 10 μL of each suspension was immediately deposited on transmission electron microscope (TEM) grids (300 mesh copper, formvar–carbon) and held for 10 min. Excess liquid was carefully removed with filter paper, and the sample was vacuum-dried for 24 h. Micrographs were obtained in a TEM Morgagni 268D (FEI Company, USA) with an acceleration voltage of 100 kV, in the Strategic Technologies Center Northeast (CETENE). The length (L) and width (D) of the BCNCs were determined from at least 100 measurements by the image analyzer, using Gimp 2.8 software.

3. Results and discussion

3.1. Zeta potential

Table 2 shows the physicochemical characterization of BC and nanocrystals obtained through acid hydrolysis under different conditions.

The zeta potential is used to evaluate the presence of surface charges. Zeta potential values with a modulus of >30 mV reflect good stability of a colloidal suspension (Mirhosseini, Tan, Hamid, & Yusof, 2008). The tested reaction conditions resulted in BCNC suspensions with high zeta potential values, confirming their stability. The nanostructures had a highly negative surface-charge density due to the conjugated sulfate groups ($-OSO_3^-$) derived from esterification of the hydroxyl groups present on the cellulose surface. Regarding the conditions evaluated, it was observed that higher H_2SO_4 concentrations and prolonged reaction times resulted in an increase in the zeta potential modulus, favoring the stability of the BCNC suspensions. However, severe reaction conditions, *e.g.* BCNC–4, can affect the polymer structure and size of the nanocrystals, thereby reducing stability.

Using a H_2SO_4 and HCl mixture (BCNC–3/HCl) resulted in a lower zeta potential compared to that observed using H_2SO_4 alone (BCNC–3) because HCl does not react with the hydroxyl groups. However, the mixture of acids produced a nanocrystal suspension with good stability due to the contributions of the sulfate groups.

3.2. TGA/DTG

TG curves and the respective DTG curves of BC and nanocrystals obtained by acid hydrolysis (Fig. 1) revealed that the mass-loss profiles were similar. Three mass-loss events can be observed during thermal analysis of the sample. The first event, occurring at approximately 50–150 °C, is attributable to the evaporation of residual water present in the material. The second event, occurring in the temperature range of 250–400 °C, is characterized by a series of reactions degradation of cellulose, including dehydration, decomposition, and depolymerization of the glycoside units. This second mass-loss event is associated with a high loss of mass of cellulosic material, which is characterized by the onset temperature (T_{Onset}). In the case of BCNC–1, BCNC–2, BCNC–3, and BCNC–4, where hydrolysis was performed with H_2SO_4 as the only acid, the degradation process was divided into 2 steps: the first step corresponded to the degradation of regions more accessible to the sulfate groups, and the second step corresponded to the breakdown of the more refractory crystalline fraction, which was less susceptible to hydrolysis. The third thermal event, which extends from 450 to 600 °C, is related to oxidation and breakdown of carbonaceous residues, yielding gaseous products of low molecular weight.

The residual mass in the TG curves for both native BC and BCNCs showed a low percentage of ashes (Table 2) when compared to PCs and PCNCs, which have ash contents ranging from 18 to 30% and

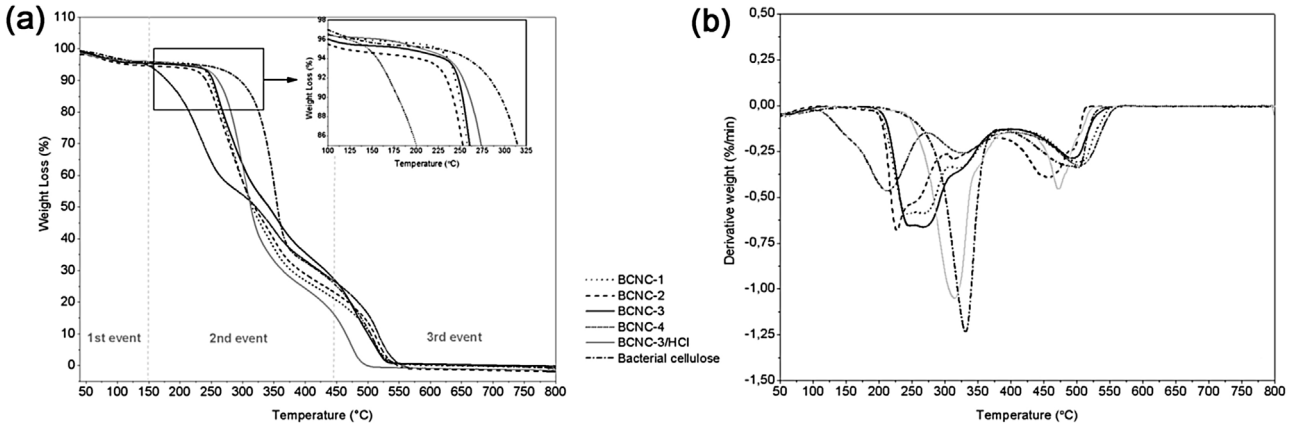

Fig. 1. TGA (a) and DTG (b) curves of native BC and BCNCs obtained through acid hydrolysis experiments performed using different concentrations of H_2SO_4 and different reaction times (BCNC–1 to BCNC–4). Combined acid hydrolysis with H_2SO_4 and HCl was also investigated (BCNC–3/HCl).

26–28%, respectively (Moriana, Vilaplana, & Ek, 2016), showing that BC exhibits much higher purity.

BC has a higher degradation temperature than PC, which shows temperature degradation between 230 and 250 °C (Guo & Catchmark, 2012; Pecoraro et al., 2008). The lower thermal stability of PC can be attributed to the presence of chemical additives that are used during the PC-extraction process.

The degradation temperature of native BC was higher than that of BCNCs. The high surface area of BCNCs may play an important role in reducing thermostability. Moreover, hydrolysis reactions with H_2SO_4 promote the formation of nanostructures with low thermal stability due to the presence of sulfate groups ($-OSO_3^-$) on the BCNC surface (Table 2). The presence of sulfate groups causes decreased activation energy for the thermal degradation of cellulose (Roman & Winter, 2004).

Considerable variation was observed between the T_{Onset} observed with the BCNC–3 and BCNC–3/HCl conditions, the former showing a higher degradation temperature. Thus, the use of HCl resulted in a T_{Onset} increase of 46 °C (17% higher), as compared with the BCNC–3 counterpart. These results agreed with data shown in the literature that combined use of H_2SO_4/HCl improves the thermal performance of CNCs due to a lower surface density of sulfate groups (Corrêa et al., 2010).

3.3. XRD

The XRD patterns of native BC and the nanocrystals showed three 2θ diffraction peaks at 14.5°, 16.4°, and 22.5°, which are usually attributed to crystallographic planes of 101 (amorphous region), 10(amorphous region), and 200 (crystalline region), respectively (Fig. 2). The presence of these 3 diffraction peaks characterizes cellulose type Iα (triclinic), which is prevalent in BC; whereas the type Iβ crystal structure (monoclinic) is found in plant cellulose (Henrique et al., 2015).

Crystallinity is a major factor that specifically influences the mechanical properties of materials. Therefore, the XRD patterns (Fig. 2) were used to determine the CrI of BC and the nanocrystals. The results showed that all BCNCs had a CrI greater than native BC (Table 2). The increase in crystallinity after acid hydrolysis reaction was due to a reduction of the amorphous content, as this region is more accessible to acid attack. Comparing the CrI of BCNC–1 and BCNC–2 (which differed in the reaction time), no significant difference was detected. However, for BCNC–4 (involving a higher H_2SO_4 concentration), a decrease in the CrI was observed, possibly due to the severe hydrolysis conditions, resulting in a likely change in the orientation of the cellulose chains. In contrast, BCNC–3/HCl showed a lower CrI than did the nanocrystals obtained after acid hydrolysis H_2SO_4 alone. This observation was potentially related to the fact that the combination of acids resulted in milder hydrolysis conditions, generating nanocrystals with higher amorphous contents.

The diffraction peaks of the crystalline phase were deconvoluted using the Pseudo–Voigt function to obtain the FWHM value. The sizes of the crystallites (CS) are shown in Table 2. Compared with the BCNC–1 and BCNC–2 conditions, the nanocrystals obtained under the BCNC–3, BCNC–4, and BCNC–3/HCl hydrolysis conditions showed slight differences in the CS values. Thus, we conclude that an H_2SO_4 concentration above 60% (w/w) and the combination of acids used in the hydrolysis reaction influence the crystalline fraction of the cellulose. For BC, the CS was higher than for the nanocrystals, suggesting that acid hydrolysis tended to degrade the crystalline fraction of the starting material. Therefore, for BC, the observed results were consistent with those by Castro et al. (2011).

After considering the results discussed above, the BCNC–1 and BCNC–3/HCl nanocrystals were selected for further study because of their stable colloidal suspensions and good thermostability. These nanocrystals were characterized chemically and morphologically by spectroscopy, calorimetry, and microscopy.

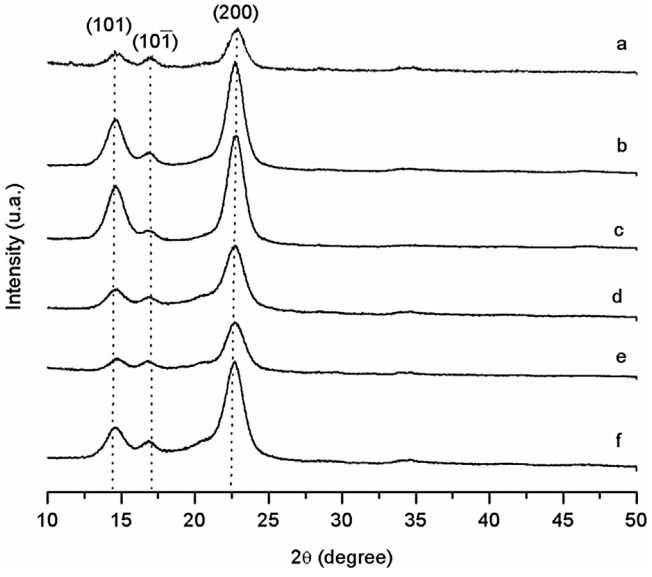

Fig. 2. XRD pattern of (a) native BC and BCNCs produced under different hydrolysis conditions, (b) BCNC–1, (c) BCNC–2, (d) BCNC–3, (e) BCNC–4, and (f) BCNC–3/HCl.

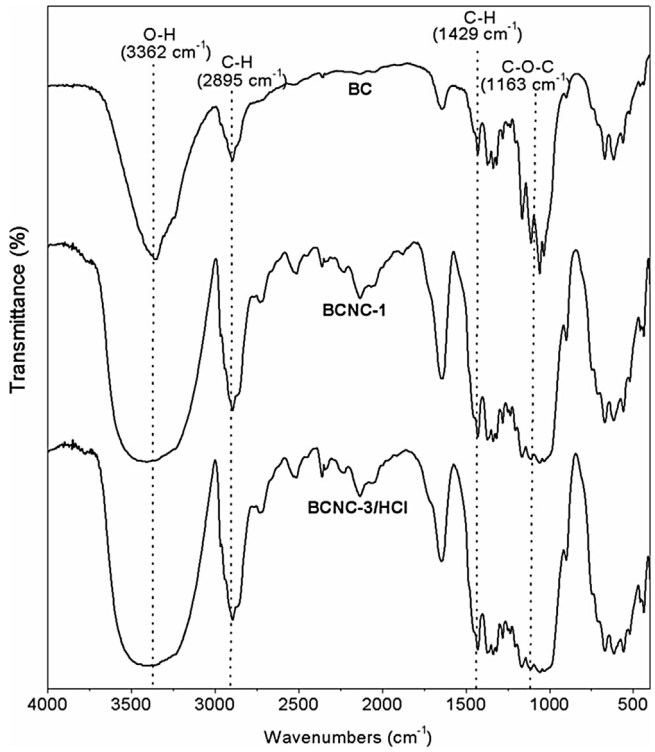

Fig. 3. FTIR spectrum of native BC and BCNCs extracted by acid hydrolysis with H_2SO_4 (BCNC–1) and with H_2SO_4/HCl combined (BCNC–3/HCl).

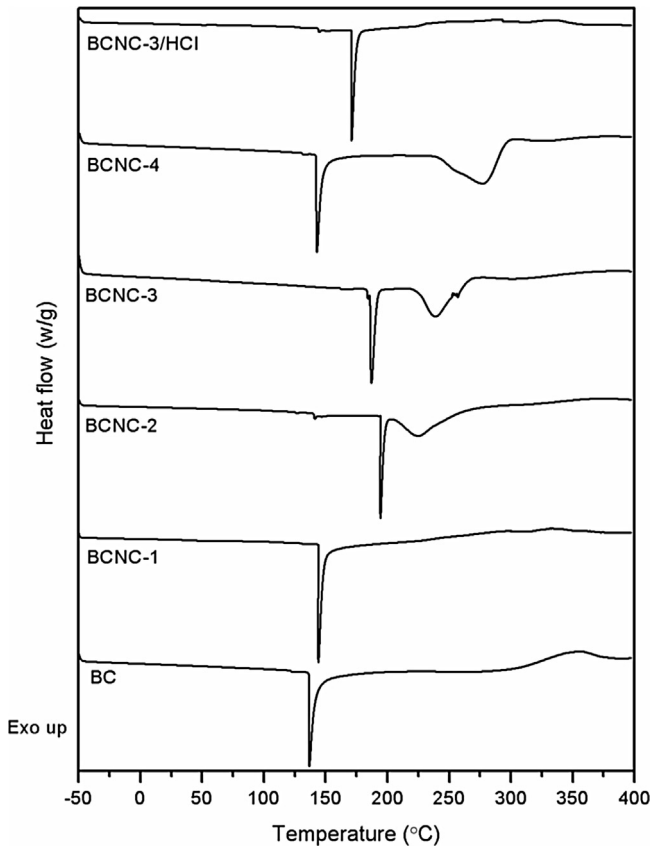

Fig. 4. DSC curve of native BC and nanocrystals obtained through acid hydrolysis performed using different H_2SO_4 concentrations and different reaction times (BCNC-1 to BCNC-4). Combined acid hydrolysis with H_2SO_4 and HCl was also investigated (BCNC-3/HCl).

3.4. FTIR

The FTIR spectra of native BC and BCNCs (Fig. 3) showed typical cellulose vibration bands, such as 3362 cm^{-1} (stretching of O—H bonds), 1429 cm^{-1} (asymmetric angular deformation of C—H bonds), 1371 cm^{-1} (symmetric angular deformation of C—H bonds), 1163 cm^{-1} (asymmetrical stretching of C—O—C glycoside bonds), 1110 cm^{-1} and 1059 cm^{-1} (stretching of C—OH and C—C—OH bonds in secondary and primary alcohols, respectively), and 897 cm^{-1} (angular deformation of C—H bonds) (Chang & Chen, 2016). Unfortunately, no 807 cm^{-1} band was observed (symmetric vibration of C—O—S bonds associated with C—O—SO_3^- groups), which are derived from esterification occurred during the hydrolysis reaction.

The FTIR spectra of PC featured vibration bands characteristic of lignin and hemicellulose, which are naturally associated with the material (Moriana, Vilaplana, & Ek, 2016). After the PC extraction/purification process, which includes delignification, bleaching, and mercerization, a change in the chemical composition of PC was observed, resulting in a spectrum with vibration bands similar to BC (Nagalakshmaiah, El Kissi, Mortha, & Dufresne, 2016). However, the PCNCs obtained by hydrolysis with H_2SO_4 and/or HCl showed chemical compositions similar to BCNCs.

3.5. DSC

Fig. 4 shows DSC thermograms of native BC and BCNCs. Calculating the endothermic peak area for cellulose decomposition provided the enthalpy-variation values of the decomposition reaction (ΔH_d). The heat-flow curves of native BC membranes showed an endothermic peak at 136.7 °C ($\Delta H = 87.72\ J\ g^{-1}$), which appeared to be the crystalline melting temperature (T_m) of the polymer. At 350.72 °C ($\Delta H_d = 86.66\ J\ g^{-1}$), an exothermic peak was followed by degradation (T_d) of the cellulosic material. Similar results were found by George et al. (2005) for BC purified via NaOH treatment. The T_m and T_d were 106.48 °C and 343.27 °C, respectively. In a study conducted by Rani, Udayasankar, & Appaiah (2011), heat-flow curves of NaOH-treated cellulose membranes showed an endothermic peak at 111.65 °C ($\Delta H = 241.8\ J\ g^{-1}$) and an exothermic peak at 369.49 °C ($\Delta H = 43.21\ J\ g^{-1}$).

For BCNCs, an endothermic peak occurred in the range of 140–195 °C and they showed enthalpy-variation values ranging from 51 to 95 $J\ g^{-1}$. Similar result was reported by Lu and Hsieh (2010), who observed more gradual thermal transitions that started at a lower temperature (approximately 150 °C). However, in the DSC curves of the BCNC–2, BCNC–3, and BCNC–4 nanocrystals, a broad endothermic event occurred between 200 and 290 °C, which was probably due to decomposition of sulfate groups and the derivative compounds, such as H_2S. In the BCNC–1 and BCNC–3/HCl curves, this endothermic peak was discrete because the nanocrystals probably had a lower sulfate content.

3.6. SEM/TEM

Fig. 5 shows BC pellicles and SEM micrographs of the dried material. The BC pellicle structure was composed of cellulose nanofibers that formed an ultrafine network, with an average width of 67.5 ± 9.4 nm, stabilized by extensive hydrogen bonding. In the study by Mohammadkazemi, Doosthoseini, Ganjian, & Azin (2015), the BC nanofibers synthesized by *Gluconacetobacter xylinus* showed an average width ranging from 22 to 80 nm, which is consistent with the results observed in this study. These nanostructures were interconnected forming a highly porous 3-dimensional structure. The characteristic nanoscale morphology of the BC promotes a high surface area and, consequently, a high water-retention capacity,

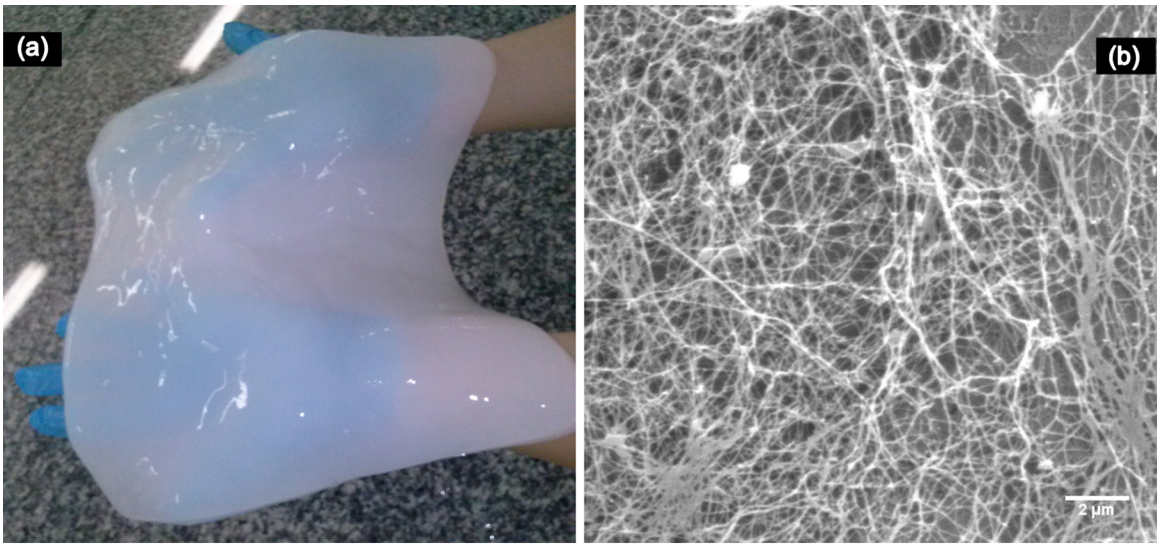

Fig. 5. Images from BCs pellicles used in this work. (a) Photograph. (b) SEM micrograph.

unlike ordinary cellulose in plants, which are approximately 100 times thicker than BC (Lai et al., 2013).

TEM micrographs of BCNC–1 and BCNC–3/HCl showed well-dispersed needle-shaped structures, an expected pattern for acid hydrolysis nanocrystals (Fig. 6).

BCNC–1 nanocrystals had a length ranging from 200 to 1000 nm and a width ranging from 16 to 50 nm, which represented an average length ($\bar{L}$) of 622 ± 100 nm and an average width ($\bar{D}$) of 33.7 ± 14 nm, corresponding to an aspect ratio (L/D) of 20.1 ± 6.6. The BCNC–3/HCl nanostructures had a length ranging from 500 to 2100 nm and a width ranging from 20 to 68 nm, corresponding to an ($\bar{L}$) of 1322 ± 189 nm, an ($\bar{D}$) of 44.3 ± 18 nm, and a ratio L/D of 21.1 ± 1.1.

The acid concentration used to hydrolyze cellulose and the ionic strength of the medium influence the morphological characteristics of the product (Dufresne, 2012). It is noteworthy that the longest nanocellulose crystals were obtained with the combined use of acids may result in crystals with a higher amorphous content, which consequently leads to a lower CrI.

Hydrolysis using high H_2SO_4 concentrations is harmful to the polymer backbone, promoting the breakage of glycosidic bonds. Yun, Cho, & Jin (2010) carried out hydrolysis reactions with H_2SO_4 at 65% (w/w) for various times (1, 2, and 3 h) and found that longer times correlated with a lower average length of BC nanocrystals and with higher sulfur contents in the nanoparticles. Therefore, acid-hydrolysis experiments performed with different H_2SO_4 concentrations (50%–65% w/w) influenced the properties of nanostructures. In addition, the use of <65% (w/w) H_2SO_4 and short reaction times (for example, BCNC–1 and BCNC–3) were more suitable for obtaining nanocrystals.

Moreover, the thermal properties resulting from the use of H_2SO_4 could be significantly improved by adding HCl to the hydrolysis reaction, without affecting the stability of the suspension or the crystallinity of the nanostructures. Thus, the combined use of acids (BCNC–3/HCl) provided nanocrystals with highly promising properties for the development of nanomaterials.

The L/D ratio of the nanocrystals is an important parameter, especially when these nanostructures are intended as a reinforcing agent in polymer matrices. In general, a ratio L/D greater than 13 promotes the formation of an anisotropic phase, resulting in improved reinforcement properties of the material (Dufresne, 2012). No considerable difference was observed between the ratio L/D of BCNC–1 and BCNC–3/HCl (20.1 ± 6.6 and 21.1 ± 1.1, respectively). These L/D values are close to those obtained by Martinez-Sanz, Lopez-Rubio, & Lagaron (2011) ($L/D = 23.33$ and 24.32), where the following conditions were used to obtain nanocrystals from BC: 50.7% (w/w) H_2SO_4, 48 h at 50 °C and 55.4% (w/w) H_2SO_4, 69 h at 50 °C, respectively. Therefore, in addition to

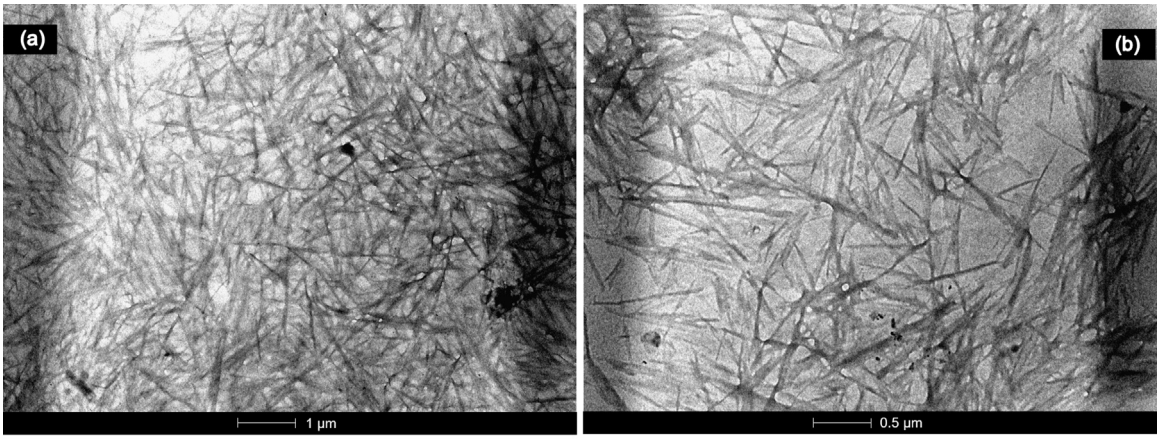

Fig. 6. TEM micrograph of BCNCs produced with (a) 50% (w/w) H_2SO_4 (BCNC–1) and (b) with a combination of H_2SO_4 and HCl (BCNC–3/HCl).

a shorter reaction time for hydrolysis, the BCNCs obtained in this study showed good *L/D* values, and thus may enable reinforcement in nanocomposites.

4. Conclusions

This work was conducted to evaluate the single and combined use of inorganic acids to obtain BCNCs. The hydrolysis reaction conditions (reaction time and type/concentration of acids) influenced the physical properties of the nanostructures, without affecting the size of the crystalline cellulose fraction. The BCNCs obtained by the combination of H_2SO_4/HCl (BCNC–3/HCl) showed good characteristics (zeta = –43.9 mV; CrI = 83%; *L/D* = 21.1; T_{Onset} = 263 °C) and the potential for application as a reinforcing agent for polymeric matrices in particular biomaterials. The combined use of acids favored the production of a promising BCNC.

Acknowledgments

The authors would like to thank Coordination for the Improvement of Higher Education Personnel (CAPES), National Counsel of Technological and Scientific Development (CNPq), and the Embrapa Tropical Agroindustry for funding this research and Strategic Technologies Center Northeast (CETENE) for supporting the transmission electron microscopy analysis.

References

Brown, A. J. (1886). On an acetic ferment which forms cellulose. *Journal of the Chemical Society, Transactions*, *49*, 432–439.
Castro, C., Zuluaga, R., Putaux, J., Caro, G., Mondragon, I., & Gañán, P. (2011). Structural characterization of bacterial cellulose produced by *Gluconacetobacter swingsii* sp. from Colombian agroindustrial wastes. *Carbohydrate Polymers*, *84*, 96–102.
Chang, W., & Chen, H. (2016). Physical properties of bacterial cellulose composites for wound dressings. *Food Hydrocolloids*, *53*, 75–83.
Charreau, H., Foresti, M. L., & Vázquez, A. (2013). Nanocellulose patents trends: A comprehensive review on patents on cellulose nanocrystals, microfibrillated and bacterial cellulose. *Recent Patents on Nanotechnology*, *7*, 56–80.
Corrêa, A. C., Teixeira, E. M., Pessan, L. A., & Mattoso, L. H. C. (2010). Cellulose nanofibers from curauá fibers. *Cellulose*, *17*, 1183–1192.
Czaja, W., Krystynowicz, A., Bielecki, S., & Brown, R. M. (2006). Microbial cellulose: The natural power to heal wounds. *Biomaterials*, *27*, 145–151.
da Silva Braid, A. C. C., de Figueirêdo, M. C. B., Matsuura, M. I. F., de Souza Filho, M. S. M., Rosa, M. F., (2015). Avaliação ambiental de nanocristais de celulose obtidos a partir de biomassa vegetal. Fortaleza: Embrapa Agroindústria Tropical – Boletim de Pesquisa e Desenvolvimento, ISSN: 1679-6543, 98, 1–30.
de figueirêdo, M. C. B., Rosa, M. F., Ugaya, C. M. L., de Souza Filho, M. S. M., da Silva Braid, A. C. C., & de Melo, L. F. L. (2012). Life cycle assessment of cellulose nanowhiskers. *Journal of Cleaner Production*, *35*, 130–139.
do Nascimento, D. M., Dias, A. F., de Araújo Junior, C. P., Rosa, M. F., Morais, J. P. S., de FIGUEIRÊDO, M. C. B., (2016). A comprehensive approach for obtaining cellulose nanocrystal from coconut fiber. Part II: Environmental assessment of technological pathways. Industrial Crops and Products. in press, 10.1016/j.indcrop.2016.02.063.
Dufresne, A. (2012). *Nanocellulose: From nature to high performance tailored materials* (1st ed.). Boston: Walter de Gruyter.
Gea, S., Reynolds, C. T., Roohpour, N., Wirjosentono, B., Soykeabkaew, N., Bilotti, E., et al. (2011). Investigation into the structural, morphological, mechanical and thermal behaviour of bacterial cellulose after a two-step purification process. *Bioresource Technology*, *102*, 9105–9110.
George, J., Ramana, K. V., Sabapathy, S. N., Jagannath, J. H., & Bawa, A. S. (2005). Characterization of chemically treated bacterial *(Acetobacter xylinum)* biopolymer: Some thermo-mechanical properties. *International Journal of Biological Macromolecules*, *37*, 189–194.
George, J., Ramana, J., Bawa, J., & Siddaramaiah, J. (2011). Bacterial cellulose nanocrystals exhibiting high thermal stability and their polymer nanocomposites. *International Journal of Biological Macromolecules*, *48*, 50–57.
Guo, J., & Catchmark, J. M. (2012). Surface area and porosity of acid hydrolyzed cellulose nanowhiskers and cellulose produced by *Gluconacetobacter xylinus*. *Carbohydrate Polymers*, *87*, 1026–1037.
Henrique, M. A., Flauzino Neto, W. P., Silvério, H. A., Martins, D. F., Gurgel, L. V. A., Barud, H. S., et al. (2015). Kinetic study of the thermal decomposition of cellulose nanocrystals with different polymorphs, cellulose I and cellulose II, extracted from different sources and using different types of acids. *Industrial Crops and Products*, *76*, 128–140.
Hu, Y., Catchmark, J. M., Zhu, Y., Abidi, N., Zhou, X., Wang, J., et al. (2014). Engineering of porous bacterial cellulose toward human fibroblasts ingrowth for tissue engineering. *Journal Material Research*, *29*, 2682–2693.
Klemm, D., Schumann, D., Udhardt, U., & Marsch, S. (2001). Bacterial synthesized cellulose – Artificial blood vessels for microsurgery. *Progress in Polymer Science*, *26*, 1561–1603.
Lai, C., Zhang, S., Sheng, L., Liao, S., Xi, T., & Zhang, Z. (2013). TEMPO-mediated oxidation of bacterial cellulose in a bromide-free system. *Colloid and Polymer Science*, *291*, 2985–2992.
Lu, P., & Hsieh, Y. (2010). Preparation and properties of cellulose nanocrystals: Rods, spheres, and network. *Carbohydrate Polymers*, *82*, 329–336.
Martínez-Sanz, M., Lopez-Rubio, A., & Lagaron, J. M. (2011). Optimization of the nanofabrication by acid hydrolysis of bacterial cellulose nanowhiskers. *Carbohydrate Polymers*, *85*, 228–236.
Mirhosseini, H., Tan, C. P., Hamid, N. S. A., & Yusof, S. (2008). Effect of Arabic gum, xanthan gum and orange oil contents on ζ-potential, conductivity, stability, size index and pH of orange beverage emulsion. *Colloids and Surfaces A: Physicochemical and Engineering Aspects*, *315*, 47–56.
Mohammadkazemi, F., Doosthoseini, K., Ganjian, E., & Azin, M. (2015). Manufacturing of bacterial nano-cellulose reinforced fiber-cement composites. *Construction and Building Materials*, *101*, 958–964.
Morais, J. P. S., Rosa, M. F., de Souza Filho, M. S. M., Nascimento, L. D., do Nascimento, D. M., & Ribeiro, A. C. (2013). Extraction and characterization of nanocellulose structures from raw cotton linter. *Carbohydrate Polymers*, *91*, 229–235.
Moreira, S., Silva, N. B., Almeida-Lima, J., Rocha, H. A. O., Medeiros, S. R., Alves, B. C., et al. (2009). BC nanofibres: In vitro study of genotoxicity and cell proliferation. *Toxicology Letters*, *189*, 235–241.
Moriana, R., Vilaplana, F., & Ek, M. (2016). Cellulose nanocrystals from forest residues as reinforcing agents for composites: A study from macro- to nano-dimensions. *Carbohydrate Polymers*, *139*, 139–149.
Nagalakshmaiah, M. E. L., Kissi, N., Mortha, G., & Dufresne, A. (2016). Structural investigation of cellulose nanocrystals extracted from chili leftover and their reinforcement in cariflex-IR rubber latex. *Carbohydrate Polymers*, *136*, 945–954.
Ng, H., Sin, L. T., Tee, T., Bee, S., Hui, D., Low, C., et al. (2015). Extraction of cellulose nanocrystals from plant sources for application as reinforcing agent in polymers. *Composites Part B: Engineering*, *75*, 176–200.
Pecoraro, E., Manzani, D., Messaddeq, Y., & Ribeiro, S. J. L. (2008). *Monomers, polymers and composites from renewable resources* (1st ed.). Oxford: Elsevier.
Pereira, A. L. S., do Nascimento, D. M., de Souza Filho, M. S. M., Morais, J. P. S., Vasconcelos, N. F., Feitosa, J. P. A., et al. (2014). Improvement of polyvinyl alcohol properties by adding nanocrystalline cellulose isolated from banana pseudostems. *Carbohydrate Polymers*, *112*, 165–172.
Qiao, C., Chen, G., Zhang, J., & Yao, J. (2016). Structure and rheological properties of cellulose nanocrystals suspension. *Food Hydrocolloids*, *55*, 19–25.
Qui, X., & Hu, S. (2013). Smart materials based on cellulose: A review of the preparations, properties, and applications. *Materials*, *6*, 738–781.
Rani, M. U., Udayasankar, K., & Appaiah, K. A. (2011). Properties of bacterial cellulose produced in grape medium by native isolate *Gluconacetobacter* sp. *Journal of Applied Polymer Science*, *120*, 2835–2841.
Roman, M., & Winter, W. T. (2004). Effect of sulfate groups from sulfuric acid hydrolysis on the thermal degradation behavior of bacterial cellulose. *Biomacromolecules*, *5*, 1671–1677.
Rosa, M. F., Medeiros, E. S., Malmonge, J. A., Gregorski, K. S., Wood, D. F., Mattoso, L. H. C., et al. (2010). Cellulose nanowhiskers from coconut husk fibers: Effect of preparation conditions on their thermal and morphological behavior. *Carbohydrate Polymers*, *81*, 83–92.
Ross, P., Mayer, R., & Benziman, M. (1991). Cellulose biosynthesis and function in bacteria. *Microbiology Reviews*, *55*, 35–58.
Segal, L., Creely, J., Martin, A., & Conrad, C. (1959). An empirical method for estimating the degree of crystallinity of native cellulose using the X-ray diffractometer. *Textile Research Journal*, *29*, 786–794.
Shah, N., U.L-Islam, M., Khattak, W. A., & Park, J. K. (2013). Overview of bacterial cellulose composites: A multipurpose advanced material. *Carbohydrate Polymers*, *98*, 1585–1598.
Svensson, A., Nicklasson, E., Harrah, T., Panilaitis, B., Kaplan, D. L., Brittberg, M., et al. (2005). Bacterial cellulose as a potential scaffold for tissue engineering of cartilage. *Biomaterials*, *26*, 419–431.
Yun, Y. S., Cho, S. Y., & Jin, H. J. (2010). Flow-induced liquid crystalline solutions prepared from aspect ratio-controlled bacterial cellulose nanowhiskers. *Molecular Crystals and Liquid Crystals*, *519*, 141–148.